Electronic Supplementary Material (ESI) for Journal of Materials Chemistry C.

Supporting Information

Engineered Current Path of Vertical Organic Phototransistors for Smart Optoelectronic Applications

Hye-Min An,[a] Hyowon Jang,[b] Hyeok Kim,[b] Sin-Doo Lee,[c] Sin-Hyung Lee*[d] and Hea-Lim Park*[a]

[a] Department of Materials Science and Engineering, Seoul National University of Science and Technology, Seoul 01811, Republic of Korea

[b] School of Electrical and Computer Engineering, Center for Smart Sensor System of Seoul(CS4), University of Seoul, 163 Seoulsiripdaero, Dongdaemun-gu, Seoul 02504, Republic of Korea

[c] School of Electrical Engineering, Seoul National University, Kwanak-gu, Seoul 151-600, Republic of Korea

[d] School of Electronics Engineering, Kyungpook National University, 80 Daehak-ro, Buk-gu, Daegu, 702-701, Republic of Korea

E-mail: sinhlee@knu.ac.kr (S.-H. Lee); parkhl21@seoultech.ac.kr (H.-L. Park)

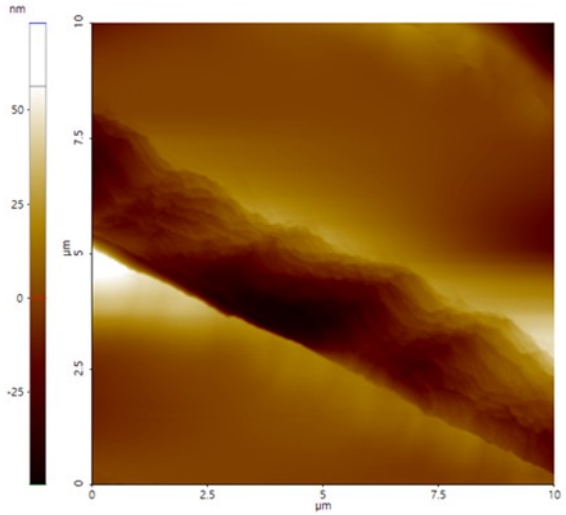

Fig. S1 AFM image of the TIPS-PEN surface used as the organic semiconducting layer.

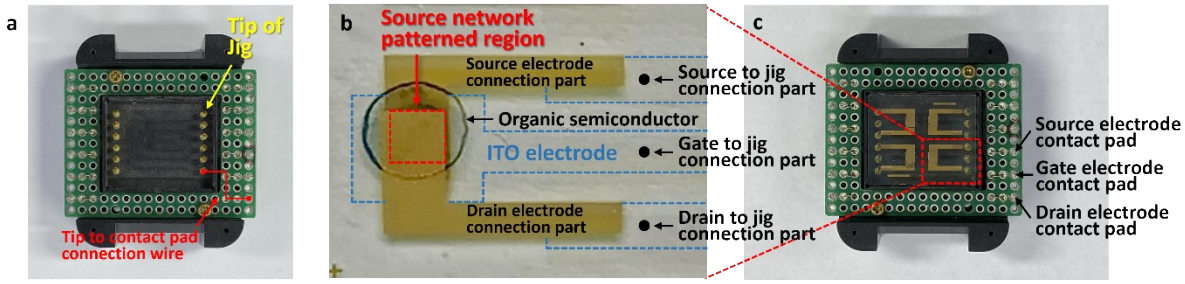

Fig. S2 Optical images of (a) a jig used for electrode connection with probe tips, (b) actual device, and (c) connected state of (a) and (b).

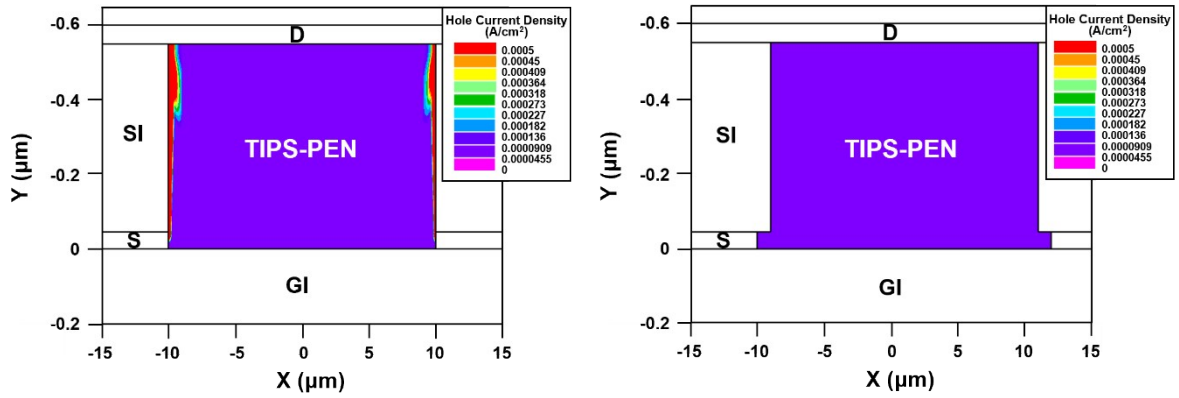

Fig. S3 Simulation results of the current-density distributions at off state ($V_D = -10$ V and $V_G = 50$ V) of the (left) typical VOPT at $t_e = 2.5$ s and (right) optimized device at $t_e = 20$ s.

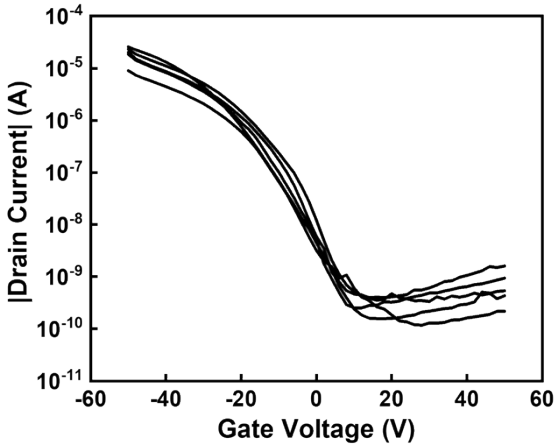

Fig. S4 Transfer curves of the optimized devices (five cells).

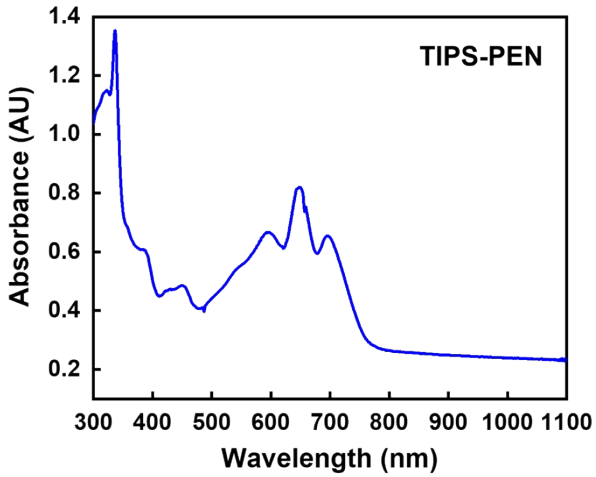

Fig. S5 Absorption spectrum of TIPS-PEN.

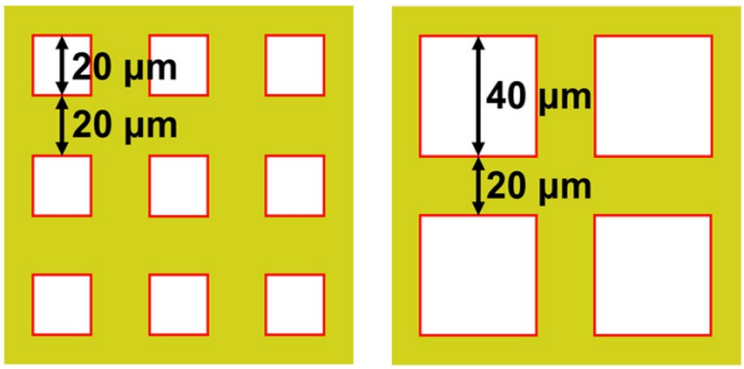

Fig. S6 Schematics of the network source electrodes of VOPTs with aperture sizes of (left) 20 and (right) 40 μm.

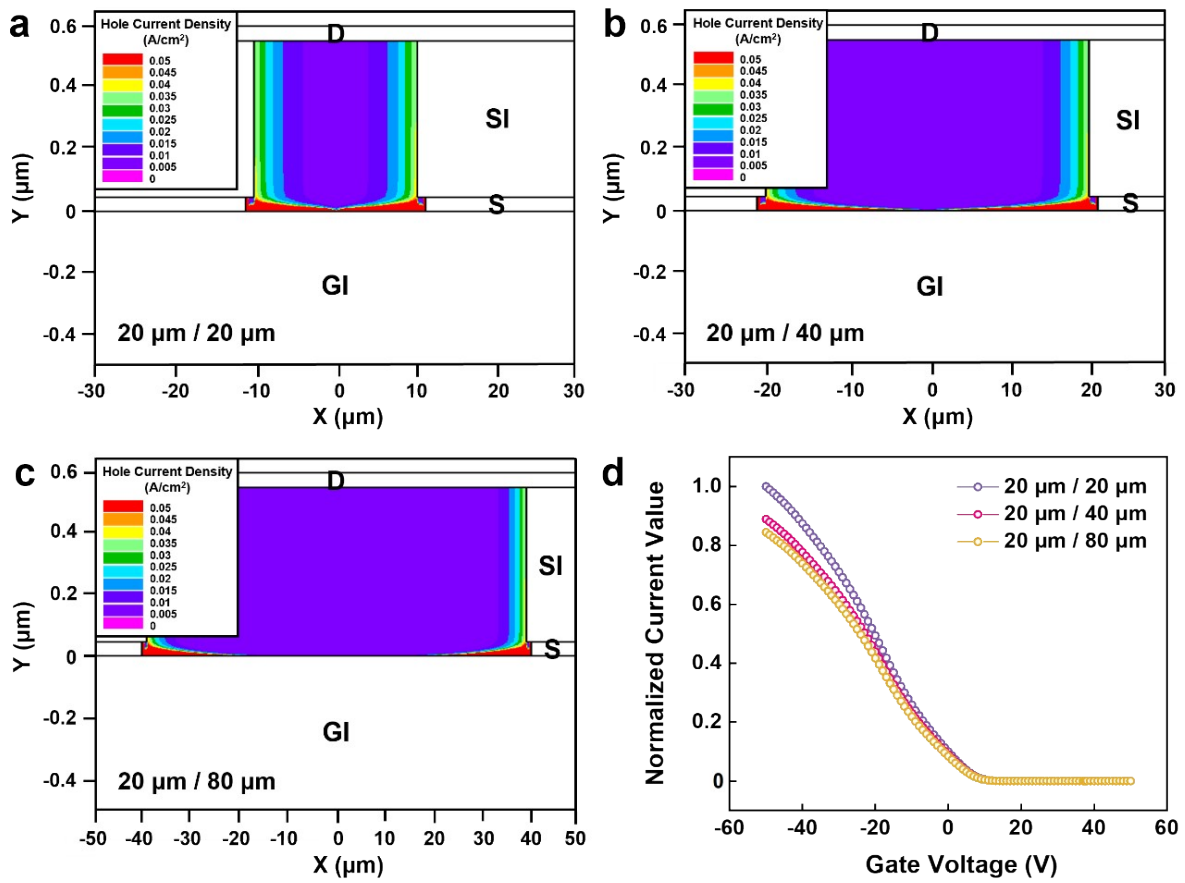

Fig. S7 Simulation results of the current-density distributions at on state (V_D = −10 V and V_G = 50 V) of VOPTs with different aperture sizes of (a) 20 μm, (b) 40 μm, and (c) 80 μm. (d) Normalized current value extracted from the simulation results of (a)–(c).

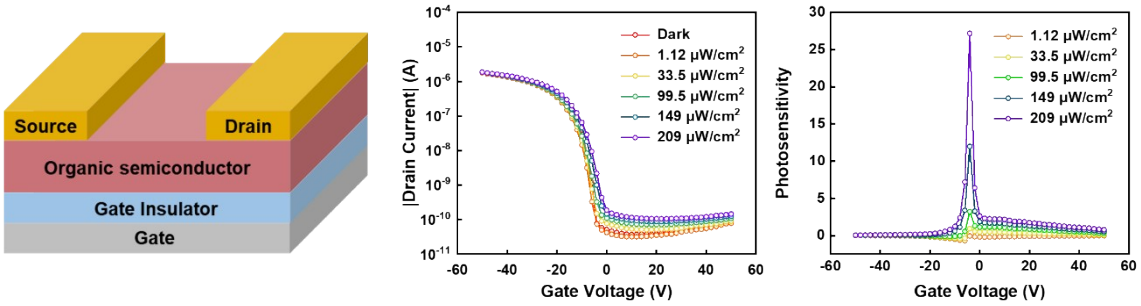

Fig. S8 (a) Schematic diagram of lateral-type OPT. (b) Static photoresponse of the lateral-type OPT under dark and illumination with various light intensities. (c) Photosensitivity values extracted from (b).

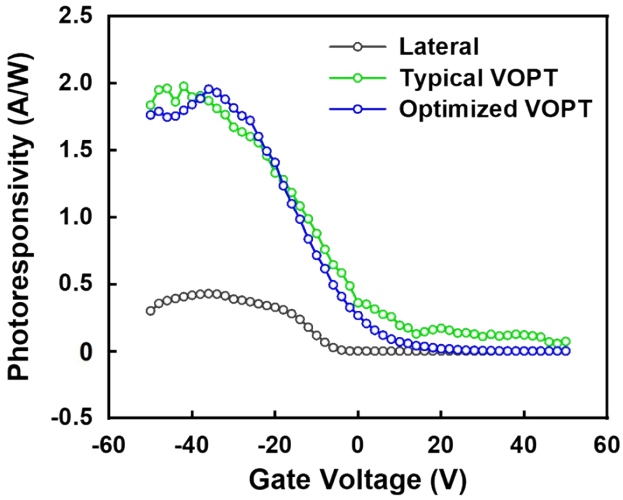

Fig. S9 Comparison of the photoresponsivities of the lateral-type OPT, vertical-type VOPT at t_e = 2.5 s (typical VOPT) and 20 s (our optimized VOPT) under a light intensity of 209 μW/cm².

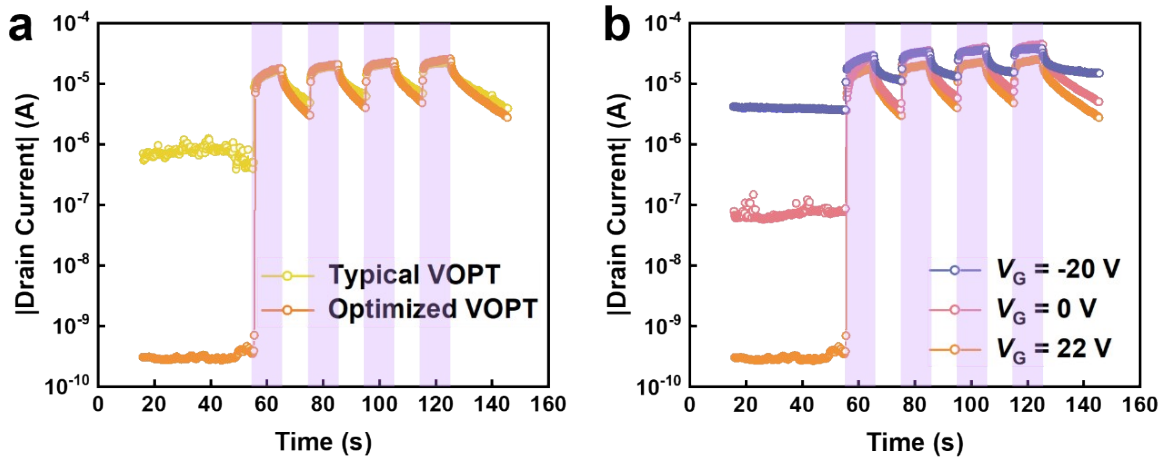

Fig. S10 Dynamic photoresponse of (a) the typical device (t_e = 2.5 s) and optimized device (t_e = 20 s) and (b) with gate voltages of −20, 0, and 22 V when multiple UV lights are applied.

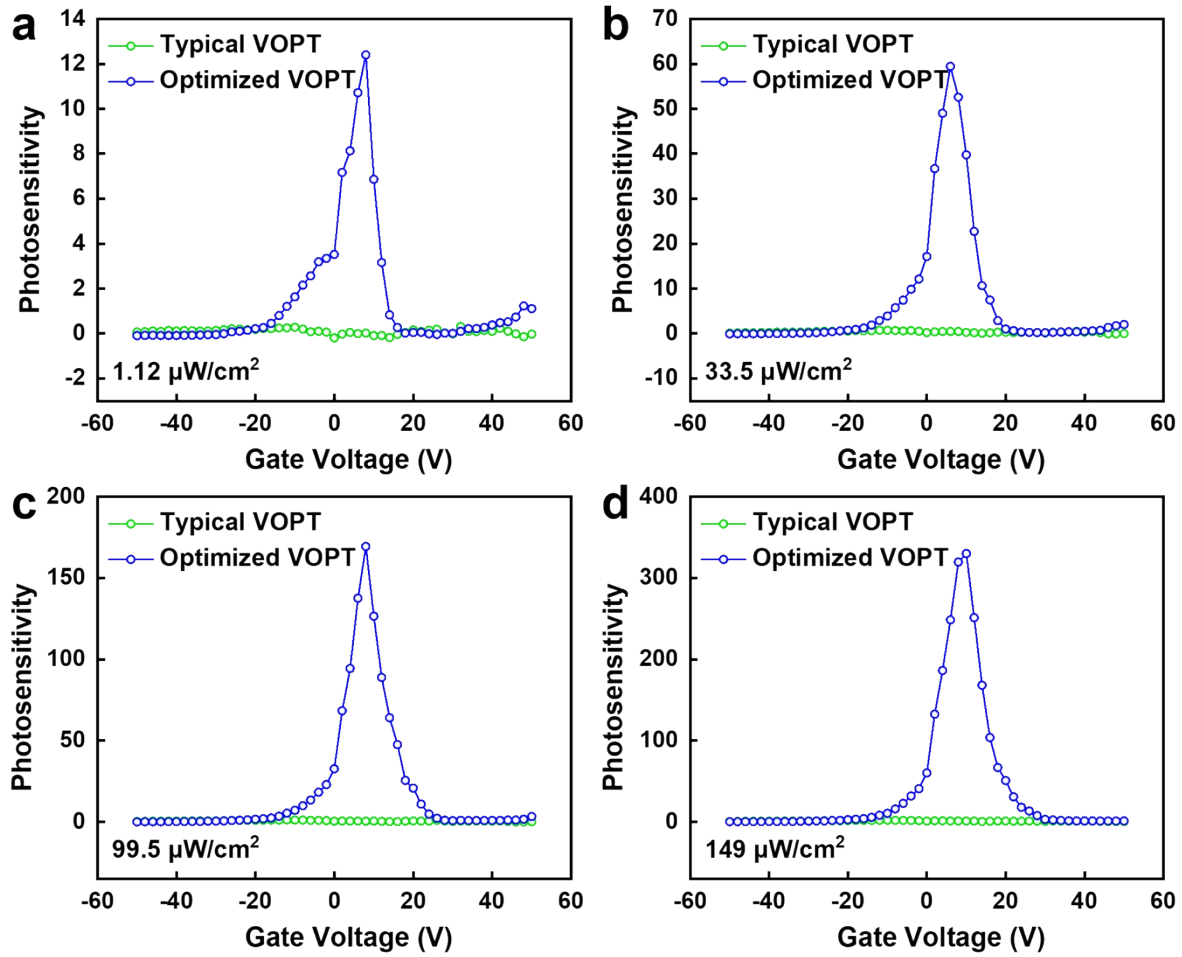

Fig. S11 Photosensitivity of the VOPTs at t_e = 2.5 s (typical VOPT) and 20 s (our VOPT) at light intensities of (a) 1.12 μW/cm^2, (b) 33.5 μW/cm^2, (c) 99.5 μW/cm^2, and (d) 149 μW/cm^2.

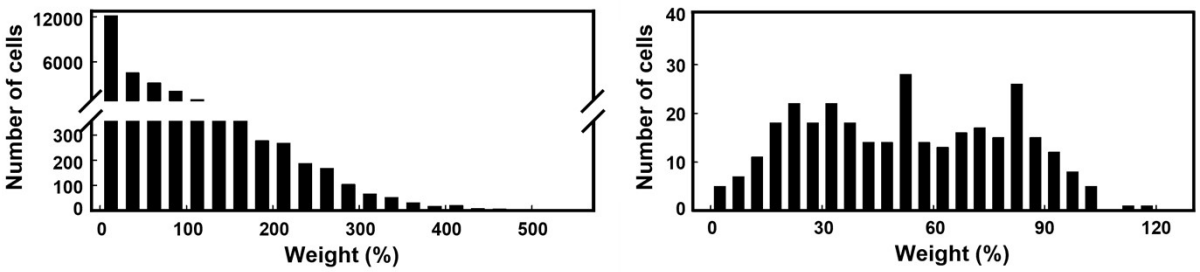

Fig. S12 Distributions of channel conductance calculated in the ideal systems.

Presence of CBL	CBL/Source pattern formation method	I_{ON}/I_{OFF} (Under dark)	Photosensitivity (Max)	Minimum light intensity ($\mu W/cm^2$)	Application	Ref.
O	Electro-beam evaporation/ Electro-beam evaporation	~10^2	~0.2	10^5	—	1
O	Laser ablation/ Thermal evaporation	~10^3	~4.5	50	—	2
O	Anodization/ Thermal evaporation	~10^3	—	—	—	3
O	Thermal evaporation/ Thermal evaporation	5.5×10^5	—	—	—	4
O	Photolithography/ Photolithography	~10^3	—	—	—	5
O	Magnetron sputtering deposition/ Thermal evaporation	~10^6	—	—	—	6
O	Photolithography/ Photolithography	~10^6	—	—	—	7
O	Evaporation/ Evaporation	~10^5	—	—	—	8
X	—/Evaporation	1.8×10^5	~10^4	50	Photo sensor	9
X	—/Spin-coating (nanowires)	~10^5	~10^5	20	Photo sensor	10
X	—/Photolithography	~5×10^2	~5×10^2	~0.57	Photo sensor	11
X	—/Spin-coating (nanowires)	~10^3	~10^2	5	Photo sensor	12
X	—/—	~5×10^2	~10	~0.15	Image sensor	13
O	Photolithography / Photolithography	~10^5	2.86×10^4	1.12	Photo sensor, photonic computing	Our device

Table S1 Summary of the characteristics of VOPTs (presence of CBL, CBL/source pattern formation method, I_{ON}/I_{OFF}, photosensitivity, minimum light intensity, and application.)

References

[1] A. Nawaz, L. Merces, D. M. de Andrade, D. H. S. de Camargo and C. C. Bof Bufon, *Nat. Commun*., 2020, **11**, 841.

[2] Z. Zhou, X. Cui, H. Zhu, C. Gu, Q. Dai, Y. Peng, S. Xu, L. Sun, W. Lv and D. Wang, *Org. Electron*., 2022, **102**, 106437.

[3] K. G. Lim, E. Guo, A. Fischer, Q. Miao, K. Leo and H. Kleemann, *Adv. Funct. Mater.*, 2020, **30**, 2001703.

[4] H. Kwon, M. Kim, H. Cho, H. Moon, J. Lee and S. Yoo, *Adv. Funct. Mater.*, 2016, **26**, 6888–6895.

[5] X. J. She, D. Gustafsson and H. Sirringhaus, *Adv. Mater.*, 2017, **29**, 1604769.

[6] A. A. Günther, M. Sawatzki, P. Formánek, D. Kasemann and K. Leo, *Adv. Funct. Mater.*, 2016, **26**, 768–775.

[7] H. Kleemann, A. A. Günther, K. Leo and B. Lüssem, *Small*, 2013, **9**, 3670–3677.

[8] D. Dahal, P. R. Paudel, V. Kaphle, R. K. Radha Krishnan and B. Lüssem, *ACS Appl. Mater. Interfaces*, 2022, **14**, 7063–7072.

[9] J. Liu, K. Zhou, J. Liu, J. Zhu, Y. Zhen, H. Dong and W. Hu, *Adv. Mater.*, 2018, **30**, 1803655.

[10] J. Zhong, X. Wu, S. Lan, Y. Fang, H. Chen and T. Guo, *ACS Photonics*, 2018, **5**, 3712–3722.

[11] Y. Yao, Q. Ou, K. Wang, H. Peng, F. Fang, Y. Shi, Y. Wang, D. I. Asperilla, Z. Shuai and P. Samorì, *Nat. Commun.*, 2021, **12**, 3667.

[12] Y. Yan, Q. Chen, X. Wang, Y. Liu, R. Yu, C. Gao, H. Chen and T. Guo, *ACS Appl. Mater. Interfaces*, 2021, **13**, 7498–7509.

[13] Y. Zhang, S. Qin, Q. Du, Y. Gan, J. Zhao, M. Li, X. Zheng, A. Wang, Y. Liu, S. Li, R. Dong, Z. Nie, C. Liu, W. Wang and F. Wang, Adv. Electron. Mater., 2023, **9**, 2201097.